https://doi.org/10.5194/nhess-2020-171
Preprint. Discussion started: 27 August 2020

Natural Hazards and Earth System Sciences
Open Access
Discussions

Multilayer-HySEA model validation for landslide generated tsunamis. Part I Rigid slides

Jorge Macías*, Cipriano Escalante, Manuel J. Castro

Departamento de Análisis Matemático, Estadística e Investigación Operativa y Matemática Aplicada, Facultad de Ciencias, Universidad de Málaga, 29080-Málaga

Abstract

The present work is devoted to the benchmarking of the Multilayer-HySEA model using laboratory experiment data for landslide generated tsunamis. This first part of the work deals with rigid slides and the second part, in a companion paper, with granular slides. The US National Tsunami Hazard and Mitigation Program (NTHMP) has proposed the experimental data used and established for the NTHMP Landslide Benchmark Workshop, held in January 2017 at Galveston. The first three benchmark problems proposed in this workshop dealt with rigid slides, simulated as a moving bottom topography, that must be imposed as a prescribed boundary condition. These three benchmarks are used here to validate the Multilayer-HySEA model. This new model of the HySEA family consists of an efficient hybrid finite volume/finite difference implementation on GPU architectures of a non-hydrostatic multilayer model. A brief description of model equations, its dispersive properties, and the numerical scheme is included. The benchmarks are described and the numerical results compared against the lab measured data for each of them. The specific aim of the present work is to validate this new code for tsunamis generated by rigid slides. Nevertheless, the overall objective of the current benchmarking effort is to produce a ready-to-use numerical tool for real world landslide generated tsunami hazard assessment. This tool has already been used to reproduce the Port Valdez Alaska 1969 event and Stromboli Italy 2002.

Keywords: Multilayer-HySEA model, tsunamis, rigid slides, model benchmarking, landslide-generated tsunamis, GPU implementation

*Corresponding author

Email address: jmacias@uma.es (Jorge Macías)

August 27, 2020

https://doi.org/10.5194/nhess-2020-171
Preprint. Discussion started: 27 August 2020

2010 MSC: 35L, 65-05, 76-05, 86-08

1. Introduction

Model development and benchmarking for earthquake-induced tsunamis is a task that has been addressed in the past and to which a lot of effort and time has been dedicated. In particular, just to mention a couple of NTHMP efforts, the 2011 Galveston benchmarking workshop (Horrillo et al., 2015) and the 2015 Portland workshop for tsunami currents (Lynett et al., 2017) were organized with this aim. However, for landslide generated tsunamis, both model development and benchmarking efforts have advanced at a slower pace. As examples of this, we can mention the 2003 NSF sponsored landslide tsunami workshop that was organized in Hawaii, and a similar follow-up workshop that took place at Catalina Island in 2006. Since then, no similar large and comprehensive benchmarking workshop has been organized (Kirby et al., 2018).

Benchmarking tsunami models is among the objectives of the NTHMP and in its 2019 Strategic Plan, the NTHMP required that all numerical tsunami inundation models to be use in hazard assessment studies in the US, should be verified as accurate and consistent through a model benchmarking process. This mandate was fulfilled in 2011, but only for seismic tsunami sources and in a limited manner for idealized solid underwater landslides. However, recent work by various NTHMP states has shown that landslide tsunami hazard may be larger than seismically-induced hazard and dominant along significant parts of the US coastline (ten Brink et al., 2014).

As a result of this need, set of candidate benchmarks were proposed to perform the required validation process. The selected benchmarks are based on a subset of available laboratory data sets for solid slide experiments and deformable slide experiments and include both submarine and subaerial slides. In order to complete this list of laboratory data, one benchmark based on a historic field event (Valdez, AK, 1964) was also selected. The EDANYA group (www.uma.es/edanya) from the University of Málaga participated in the work-

https://doi.org/10.5194/nhess-2020-171
Preprint. Discussion started: 27 August 2020

shop that was organized at Texas A&M University - Galveston, on January 9-11, 2017, presenting results for the benchmarking tests with two numerical codes: Landslide-HySEA and Multilayer-HySEA models. At Galveston, we presented numerical results for six out of the seven benchmark problems proposed, including the field case. The present work aims at presenting the numerical results obtained for the Multilayer-HySEA model in the framework of the validation effort described above for the case of rigid slide generated tsunamis. The benchmark problems dealing with granular slides are presented in the companion paper Macías et al. (2020a). A summary of the results for the field case at Port Valdez can be found at Macías et al. (2017).

Twenty years ago, at the beginning of the century, solid block landslide modeling challenged researchers and was undertaken by a number of authors (Grilli and Watts, 1999, 2005; Grilli et al., 2002; Lynett and Liu, 2002; Watts et al., 2003; Wu, 2004; Watts et al., 2005; Liu et al., 2005) and laboratory experiments were developed for those cases and for tsunami model benchmarking (Enet and Grilli, 2007) (see also Ataie-Ashtiani and Najafi-Jilani (2008)). The benchmark problems performed in the present work are based on the laboratory experiments of Grilli and Watts (2005) for BP1, Enet and Grilli (2007) for BP2, and Wu (2004); Liu et al. (2005) for BP3. The basic reference for these three benchmarks, but also the three ones related to granular slides and the Alaska field case, all of them proposed by the NTHMP, is Kirby et al. (2018). We highly recommend checking this reference for further details on benchmark descriptions, data provided for performing them, required benchmark items, and inter-model comparison. Finally, we want to stress that the ultimate goal of the present benchmarking effort is to provide the tsunami community with a model NTHMP-approved for landslide generated tsunami hazard assessment, similarly as we did with the Tsunami-HySEA model for the case of earthquake-generated tsunamis (Macías et al., 2017; Macías et al., 2020c,d).

https://doi.org/10.5194/nhess-2020-171
Preprint. Discussion started: 27 August 2020

Natural Hazards and Earth System Sciences
Discussions

2. HySEA models for landslide generated tsunamis

The HySEA (Hyperbolic Systems and Efficient Algorithms) software consists of a family of geophysical codes based on either single layer, two-layer stratified systems or multilayer shallow water models. HySEA codes[1] have been developed by the EDANYA Group from UMA (the University of Malaga) for more than a decade. These codes are in continuous development, evolution and upgrading and everyday they are serving to a wider scientific community. The first model we developed dealing with landslide-generated tsunamis, consisted in a stratified two-layer Savage-Hutter shallow water model, the Landslide-HySEA model. It was implemented based on the model described in Fernández et al. (2008) and it was incorporated to the HySEA family. A first validation of this code, comparing numerical results with the laboratory experiments of Heller and Hager (2011) and Fritz et al. (2001) can be found at Sánchez-Linares (2011). In 2018, the numerical simulation of the Lituya Bay 1958 mega-tsunami with real topo-bathymetric data and encouraging results (González-Vida et al., 2019), represented a milestone in the verification process of this code. This validation effort was undertaken under a research contract with PMEL/NOAA. The result of this project leads to NCTR (NOAA Center for Tsunami Research) to adopt Landslide-HySEA as the numerical code used to the generate initial conditions for the MOST model to be initialized in the case of landslide-generated tsunami scenario to be simulated. Further applications of Landslide-HySEA can be found at de la Asunción et al. (2013), Macías et al. (2015), and Iglesias (2015).

The waves generated in the laboratory tests proposed in the NTHMP selected benchmarks are high frequency and dispersive, and the generated flows have a complex vertical structure. Thus, the numerical model used must be able to reproduce such effects. This makes it not suitable to use the two-layer Landslide-HySEA model to reproduce these experimental results as non-

[1] https://edanya.uma.es/hysea

https://doi.org/10.5194/nhess-2020-171
Preprint. Discussion started: 27 August 2020

hydrostatic effects and a richer vertical structure is required. Attending to these requirements, the Multilayer-HySEA model was very recently implemented, considering a stratified structure in the simulated fluid and including non-hydrostatic terms. The multilayer model is able to take into account the full vertical structure (2D for BP1 and BP2) and 3D (for BP3).

3. Model Equations

The Multilayer-HySEA model implements one of the multilayer non-hydrostatic models of the family introduced and described in Fernández-Nieto et al. (2018) The governing equations, that are obtained by a process of depth-averaging, correspond to a semi-discretization for the vertical variable of the Euler equations. The total pressure is decomposed into a sum of hydrostatic and non-hydrostatic pressures. The horizontal and vertical velocities are assumed to have a constant vertical profile. The proposed model admits an exact energy balance and, when the number of layers increases, the linear dispersion relation of the linear model converges to the same of Airy's theory (Fernández-Nieto et al., 2018). The model proposed in Fernández-Nieto et al. (2018) can be written in a compact form as:

$$\left\{\begin{array}{l}\partial_t h + \partial_x (hu) = 0,\\[2ex] \partial_t (hu_\alpha) + \partial_x \left(hu_\alpha^2 + \dfrac{1}{2}gh^2\right) - gh\partial_x H + u_{\alpha+1/2}\Gamma_{\alpha+1/2} - u_{\alpha-1/2}\Gamma_{\alpha-1/2} = \\ \qquad\qquad\qquad - h\left(\partial_x p_\alpha + \sigma_\alpha \partial_z p_\alpha\right) - \tau,\\[2ex] \partial_t (hw_\alpha) + \partial_x (hu_\alpha w_\alpha) + w_{\alpha+1/2}\Gamma_{\alpha+1/2} - w_{\alpha-1/2}\Gamma_{\alpha-1/2} = -h\partial_z p_\alpha,\\[2ex] \partial_x u_{\alpha-1/2} + \sigma_{\alpha-1/2}\partial_z u_{\alpha-1/2} + \partial_z w_{\alpha-1/2} = 0,\end{array}\right. \tag{1}$$

where, for $\alpha \in \{1,\ 2, \ldots, L\}$, the following notation is used:

https://doi.org/10.5194/nhess-2020-171
Preprint. Discussion started: 27 August 2020

Natural Hazards and Earth System Sciences
Discussions

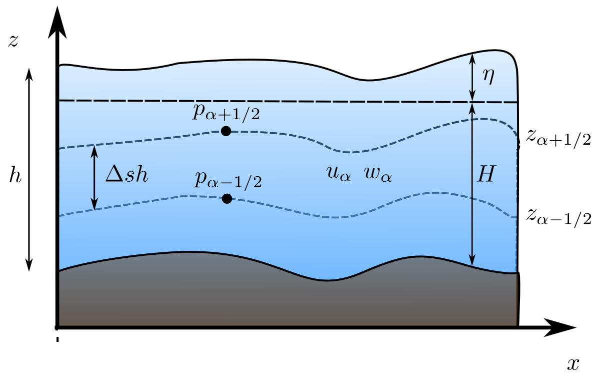

Figure 1: Schematic diagram describing the multilayer system

$$f_{\alpha+1/2} = \frac{1}{2}\left(f_{\alpha+1} + f_\alpha\right), \ \partial_z f_{\alpha+1/2} = \frac{1}{h\Delta s}\left(f_{\alpha+1} - f_\alpha\right),$$

where f denotes one of the generic variables of the system, i.e., u, w and p, and, finally,

$$\sigma_\alpha = \partial_x\left(H - h\Delta s(\alpha - 1/2)\right), \ \sigma_{\alpha-1/2} = \partial_x\left(H - h\Delta s(\alpha - 1)\right).$$

Total depth, h, is split along the vertical axis into $L \geq 1$ layers and $\Delta s = 1/L$ (see Figure 1). The variables u_α and w_α are the depth-averaged velocities in the x and z directions, respectively, t is time and g is gravitational acceleration. The non-hydrostatic pressure at the interface $z_{\alpha+1/2}$ is denoted by $p_{\alpha+1/2}$. The water surface elevation measured from the still-water level is $\eta = h - H$, where H is the water depth when the water is at rest. Finally, τ is a friction law term, and the terms $\Gamma_{\alpha+1/2}$ account for the mass transfer across interfaces and are defined by

$$\Gamma_{\alpha+1/2} = \sum_{\beta=\alpha+1}^{L} \partial_x\left(h\Delta s\left(u_\beta - \bar{u}\right)\right), \ \bar{u} = \sum_{\alpha=1}^{L} \Delta s u_\alpha$$

In order to close the system of equations, the following boundary conditions are considered

$$p_{L+1/2} = 0, \ u_0 = 0, \ w_0 = -\partial_t H.$$

https://doi.org/10.5194/nhess-2020-171
Preprint. Discussion started: 27 August 2020

Note that the motion of the bottom surface can be taken into account as a boundary condition, imposing $w_0 \neq 0$. Therefore, this model can simulate the interaction with a slide in the case that the motion of the bottom is prescribed by a function, given by a set of data, or simulated by a numerical model. In the present study, we are going to consider tests where the motion of the seafloor is given by a known function (the solid moving block).

3.1. Linear dispersion relation

Some dispersive properties of the system (1) are presented in this subsection, in particular, the phase and group velocities, and the linear shoaling. The first two properties are related to the propagation of dispersive wave trains and the last one to shoaling processes.

To obtain such properties, the system (1) is linearised around the water at rest steady-state solution. After that, a Stokes-type Fourier analysis is carried out looking for first-order planar wave solutions. This method constitutes a standard procedure to study systems that model dispersive water waves (see Escalante et al. (2018a); Lynett and Liu (2004); Madsen and Sorensen (1992); Schäffer and Madsen (1995) and references therein). The phase and group velocities as well as the linear shoaling gradient are, respectively, defined as:

$$C = \omega/k, \quad G = C + k\partial_k C, \quad \frac{\partial_x \eta}{\eta} = -\gamma \frac{\partial_x H}{H},$$

where ω denotes the angular frequency, k the local wave-number and H the typical depth.

The measured quantities C, G and γ are solely functions of the local wave-number and the typical depth H. Thus, one can obtain the so-called linear dispersion relation of the three measured quantities. From the Airy wave theory, one can also obtain the corresponding linear dispersion relations that state the linear theory for the considered quantities (see Schäffer and Madsen (1995) for the Airy reference formulae).

The expressions of the phase velocity for the system (1) are given in Table 1 for the non-linear hydrostatic shallow water system (SWE) and the Multilayer-

https://doi.org/10.5194/nhess-2020-171
Preprint. Discussion started: 27 August 2020

HySEA (non-hydrostatic) system with $j \geq 1$ layers (NH–jL). The last two columns contain $Er_C(s)$ for $s = 5$ and $s = 5$, where $Er_C(s)$ represents the maximum relative error of the phase velocity with respect to the Airy in a range $kH \in [0, s]$ in percent, i.e.:

$$Er_C(s) = 100 \cdot \max_{kH \in [0,s]} \left(\frac{|C(kH) - C(kH)_{Airy}|}{|C(kH)_{Airy}|} \right).$$

Multilayer System – Phase velocity – Errors for kH up to 5 and 15			
Model	Phase velocity	$Er_C(5)$	$Er_C(15)$
(SWE)	gH	73.63 %	123.61 %
(NH-1L)	$gH \dfrac{1}{1 + \frac{1}{4}(kH)^2}$	3.02 %	16.95 %
(NH-2L)	$gH \dfrac{1 + \frac{(kH)^2}{16}}{1 + \frac{3(kH)^2}{8} + \frac{(kH)^4}{256}}$	0.71 %	10.67 %
(NH-3L)	$\dfrac{1 + \frac{5(kH)^2}{54} + \frac{(kH)^4}{1296}}{1 + \frac{5(kH)^2}{12} + \frac{5(kH)^4}{432} + \frac{1(kH)^6}{46656}}$	0.31 %	0.62 %
(NH-5L)	$\dfrac{1 + \frac{3(kH)^2}{25} + \frac{63(kH)^4}{2510^3} + \frac{3(kH)^6}{2510^4} + \frac{(kH)^8}{1010^7}}{1 + \frac{9(kH)^2}{20} + \frac{21(kH)^4}{1010^2} + \frac{21(kH)^6}{1010^4} + \frac{9(kH)^8}{2010^6} + \frac{(kH)^{10}}{1010^9}}$	0.11 %	0.11 %

Table 1: Phase velocity expressions and maximum of the relative error $Er_C(s)$ compared with the Airy's theory for different ranges of $kH \in [0, s]$ for the non-linear hydrostatic shallow water system (SWE) and the Multilayer-HySEA (non-hydrostatic) system with $j \geq 1$ layers (NH–jL).

The main goal when deriving dispersive shallow water systems is to get the

https://doi.org/10.5194/nhess-2020-171
Preprint. Discussion started: 27 August 2020

most accurate dispersive relations as possible, compared with the Airy wave theory, without highly increasing the complexity of the system. See Schäffer and Madsen (1995) for a review on state-of-the-art or a two-layer with improved dispersive relations in Lynett and Liu (2004), and an enhanced two-layer non-hydrostatic pressure system in Escalante et al. (2018a). It has been shown (Fernández-Nieto et al., 2018), that increasing the number of layers leads to the convergence of the linear dispersion relation of the linear model to the same of Airy's theory. Figure 2 shows this behavior and highlights the huge discrepancies between the Airy's theory and the systems (SWE) and (NH-1L). It is well known that waves generated by landslides, might present high characteristic values for kH. For the (SWE) system, it is well known that it has an accurate phase velocity in a small range of kH, and that this system is appropriate for long waves as tsunami waves, but not for dispersive waves with higher values of kH. In the same vein, the one layer non-hydrostatic pressure system (NH-1L) can improve these results, but again, poor linear dispersive results are achieved in a range of kH between 5 and 15. However, when the number of layers, L, is set to 3 (still a small value) the system (1) is in an excellent agreement with the Airy theory for kH up to 15. For the phase celerity, the percentage error is less than 0.62%, and for the group velocity is less than 1% for kH smaller than 10 (see Figure 2). Linear shoaling is also well reproduced in this same range.

The Multilayer-HySEA model presents enhanced dispersive properties. In order to have similar dispersive results as the ones obtained here using a three-layer system, at least five layers are required for other similar multilayer models as the one presented in Bai and Cheung (2018). Furthermore, the results presented for the phase velocity with two layers in Table 1 shows that the system proposed here produces smaller relative error for kH up to 15 compared with the two-layer system in Cui et al. (2014). That means that the Multilayer-HySEA model can achieve better dispersive properties than models having similar or even more computational complexity.

https://doi.org/10.5194/nhess-2020-171
Preprint. Discussion started: 27 August 2020

Natural Hazards and Earth System Sciences
Discussions

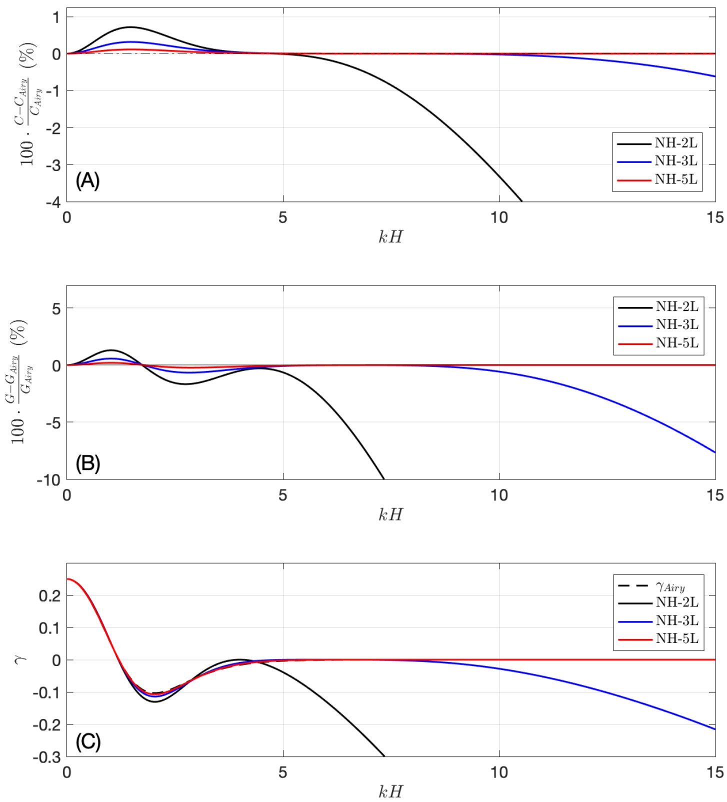

Figure 2: Relative error for the phase velocities (A), the group velocities (B), and comparison with the reference shoaling gradient (C), with respect to the Airy theory for the described multilayer systems.

4. Numerical Solution Method

The discretization of system (1) is performed following the natural extension of the procedure described in Escalante et al. (2018a,b) for the one and two layer non-hydrostatic system, where a splitting technique has been proposed.

The non-conservative hyperbolic underlying system (1) given by the compact

https://doi.org/10.5194/nhess-2020-171
Preprint. Discussion started: 27 August 2020

equation

$$\partial_t \mathbf{U} + \partial_x \mathbf{F}_{SW}(\mathbf{U}) + \mathbf{B}_{SW}(\mathbf{U})\partial_x \mathbf{U} = \mathbf{G}_{SW}(\mathbf{U})\partial_x H \tag{2}$$

is discretized using a second order finite volume PVM positive-preserving well-balanced path-conservative method (Fernández-Nieto et al., 2011), where the following compact notation has been used:

$$\mathbf{U} = \begin{pmatrix} h \\ hu_1 \\ \vdots \\ hu_L \\ hw_1 \\ \vdots \\ hw_L \end{pmatrix}, \ \mathbf{F}_{SW}(\mathbf{U}) = \begin{pmatrix} hu \\ \dfrac{hu_1^2}{h} + \dfrac{1}{2}gh^2 \\ \vdots \\ \dfrac{hu_L^2}{h} + \dfrac{1}{2}gh^2 \\ hu_1w_1 \\ \vdots \\ hu_Lw_L \end{pmatrix}, \ \mathbf{G}_{SW}(\mathbf{U}) = \begin{pmatrix} 0 \\ gh \\ \vdots \\ gh \\ 0 \\ \vdots \\ 0 \end{pmatrix}.$$

and $\mathbf{B}_{SW}$ is a matrix such $\mathbf{B}_{SW}\partial_x \mathbf{U}$ contains the non-conservative products related to the mass transfer across interfaces appearing at the momentum equations.

Next, the non-hydrostatic pressure vector term $\mathcal{T}_{\mathcal{NH}}(h, \partial_x h, H, \partial_x H, p, \partial_x p)$ given by

$$\mathcal{T}_{\mathcal{NH}}(h, \partial_x h, H, \partial_x H, p, \partial_x p) = -\begin{pmatrix} 0 \\ h\left(\partial_x p_1 + \sigma_1 \partial_z p_1\right) \\ \vdots \\ h\left(\partial_x p_L + \sigma_L \partial_z p_L\right) \\ h\partial_z p_1 \\ \vdots \\ h\partial_z p_L \end{pmatrix},$$

is computed solving an elliptic operator that appears when imposing the conti-

https://doi.org/10.5194/nhess-2020-171
Preprint. Discussion started: 27 August 2020

Natural Hazards and Earth System Sciences
Open Access
Discussions

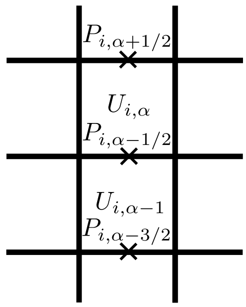

Figure 3: Arragement of discrete variables in the multilayer model discretization algorithm

nuity equation at each layer, $\mathcal{B}(\mathbf{U}, \partial_x \mathbf{U}, H, \partial_x H) = 0$, where

$$\mathcal{B}(\mathbf{U}, \partial_x \mathbf{U}, H, \partial_x H) = \begin{pmatrix} \partial_x u_{1/2} + \sigma_{1/2} \partial_z u_{1/2} + \partial_z w_{1/2} \\ \vdots \\ \partial_x u_{L-1/2} + \sigma_{L-1/2} \partial_z u_{L-1/2} + \partial_z w_{L-1/2} \end{pmatrix}.$$

The elliptic operator is discretized using standard central finite differences. Let us also point out that a common arrangement of the discretized variables is used (see Figure 3). The resulting linear system is solved using an iterative Jacobi method combined with a scheduled relaxation (see Adsuara et al. (2016); Escalante et al. (2018a,b)).

Finally, when the pressure corrections are computed, the discharges at each layer are updated. The resulting numerical scheme is well-balanced for the water at rest solution and is linearly L^∞-stable under the usual CFL condition related to the hydrostatic system. It is also worth mentioning that the numerical scheme is positive preserving and can deal with emerging topographies. Finally, its extension to 2D is straightforward. In this case, the computational domain is decomposed into subsets with a simple geometry, called cells or finite volumes. The numerical algorithm is well suited for its implementation in GPU architectures, as is shown in Castro et al. (2011). Furthermore, the compactness of the numerical stencil and the natural and the massively parallelization of the Jacobi method makes it possible that the second step can also be implemented

https://doi.org/10.5194/nhess-2020-171
Preprint. Discussion started: 27 August 2020

in GPUs (see Escalante et al. (2018b,a)). That results in a high efficiency of the numerical code and much shorter computational times.

5. Benchmark Problem Comparisons

In this Section, the numerical results obtained with the Multilayer-HySEA model and the comparison with the measured lab data for waves generated by the movement of a rigid bottom surface or of a solid block are presented. In particular, BP1 deals with a 2D submarine solid slide, BP2 with a 3D submarine slide and, finally, BP3 consists of two 3D slides, one partially submerged and a second one representing a completely submarine slide. In all these cases, a moving bottom condition has been used to model the solid block movement. The description of all these benchmarks can be found at LTMBW (2017) and Kirby et al. (2018).

5.1. Benchmark Problem 1: Two-dimensional submarine solid block

This benchmark problem is based on the 2D laboratory experiments of Grilli and Watts (2005) which were performed at the University of Rhode Island. Refer to the above-mentioned work to get a detailed description of the present benchmark. Figure 4 depicts the sketch of the laboratory experiment design. The 2D slide model is semi-elliptical, lead-loaded, and rolling down a smooth

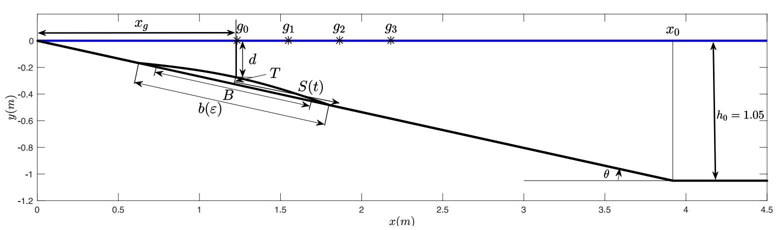

Figure 4: BP1. Sketch of main parameters and variables for wave generation by 2D rigid slide. [Modified from Grilli and Watts, 2005].

slope with a slope angle $\theta = 15°$ (2 mm above the slope), in between two vertical side walls, 20 cm apart. The water depth is $h_0 = 1.05$ m over the flat bottom

https://doi.org/10.5194/nhess-2020-171
Preprint. Discussion started: 27 August 2020

part. The slide dimensions were, length B = 1 m, maximum thickness $T = T_{\text{ref}}$ $= 0.052$ m, and width $w = 0.2$ m. The model initial submergence d was varied in experiments and the free surface elevation recorded at 4 capacitance wave gauges installed at locations: $x' = 1.175$, 1.475, 1.775, and 2.075 m, the first location being nearly identical to $x'_g = 1.168$ m (where de tilde variables, as x', mean than non-dimensional units are used -see Table 3-).

x'_g	T'	d'	θ	B	$b(\epsilon)$
1.168	0.052	0.259	15	1	1.225

Table 2: Values for variables defining setup configuration.

	g_0	g_1	g_2	g_3
x	1.234	1.549	1.864	2.179
$x' = x/h_0$	1.175	1.475	1.775	2.075

Table 3: Gauge positions in dimensional and non-dimensional units.

In this benchmark, two items remained not completely determined in the original description provided: the first one is related with the initialization of the numerical experiment, the second one is related with how and where the solid moving block must stop. Other small issues related to the description of the benchmark were put forward in Macías et al. (2017) at our NTHMP report.

The motion of the rigid slide was prescribed as a function of time as

$$S(t) = S_0 \log(\cosh(t/t_0))$$

where $S_0 = u_t^2/a_0 = 2.110$ m, $t_0 = u_t/a_0 = 1.677$ s, $a_0 = 0.75$ m/s^2 and $u_t = 1.258$ m/s is the terminal velocity. Figure 5 shows the prescribed acceleration, velocity and rigid slide displacement.

The benchmark here consists of using the above information on slide shape, submergence, and kinematics, together with reproducing the experimental set-up to simulate surface elevations measured at the four wave gauges (average of 2 replicates of experiments provided).

https://doi.org/10.5194/nhess-2020-171
Preprint. Discussion started: 27 August 2020

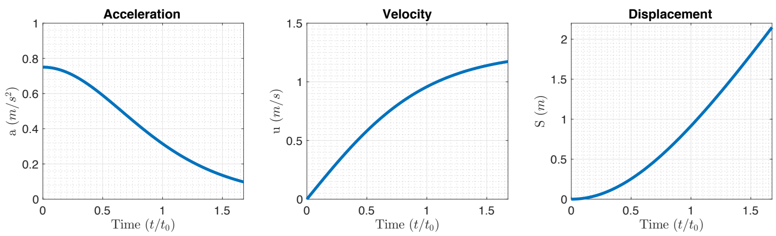

Figure 5: BP1. Prescribed acceleration, velocity and displacement of the solid slide.

Then, in order to reproduce the lab experiment, the interval $[-1, 10]$ discretized with $\Delta x = 0.02\ m$, is the computational domain considered. In the vertical, taking three layers seems to produce optimal results. Increasing the number of layers gives similar results increasing the computational cost. The stability CFL number was set to 0.9 and $g = 9.81$. The numerical simulation performed was 4 s long in real time. At the open boundaries, free outflow conditions were imposed. In order to capture turbulent processes, the complete Navier-Stokes viscous stress tensor is used (Ma et al., 2012). The turbulent kinematic viscosity is estimated using the Smagorinsky subgrid model, with $C_s = 0.2$ (Smagorinsky turbulent coefficient) and $k_s = 0.01$ (bottom roughness height).

In Figure 6 the comparison of the numerical results with the filtered lab measured data is presented. An excellent overall agreement between them can be observed. Some discrepancies can be seen after draw-down in all the gauges. This behavior could also be observed, except for the last gauge, at Grilli and Watts (2005) results. These authors explained that this behavior could be due to unwanted surface tension effects. Given this comparison, and considering the experimental variations and errors inherent to laboratory work and data processing, it can be concluded that the Multilayer-HySEA model performs optimally the present benchmark test.

https://doi.org/10.5194/nhess-2020-171
Preprint. Discussion started: 27 August 2020

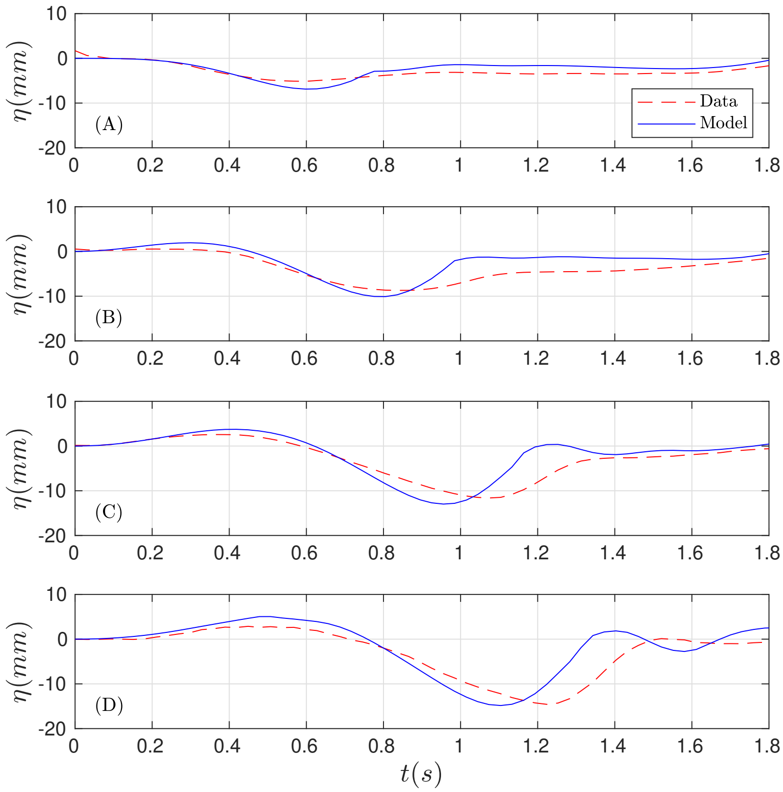

Figure 6: BP1. Filtered data (in red) and numerically simulated (in blue) time series at wave gauges (A) g_0, (B) g_1, (C) g_2, and (D) g_3.

5.2. Benchmark Problem 2: Three-dimensional submarine solid block

This second benchmark consists of a 3D extension of BP1. The longitudinal sketch of the experiment is the same as in Figure 4. In the horizontal plane, cross-sections are elliptic, the plan view of the rigid slide, for the case $d = 61\,mm$, is presented in Figure 7. It is based on the 3D laboratory experiments of Enet and Grilli (2007). The experiments were also performed at the University of Rhode Island in a water wave tank of width 3.6 m and length 30 m, with a still water depth of 1.5 m over the flat bottom portion. As in the previous benchmark, the angle of the plane slope where the slide slid down is $\theta = 15°$. The submarine

https://doi.org/10.5194/nhess-2020-171
Preprint. Discussion started: 27 August 2020

Natural Hazards and Earth System Sciences
Discussions

slide model was built as a streamline Gaussian-shaped aluminum body with elliptical footprint (see Figure 7), with down-slope length $b = 0.395\,\mathrm{m}$, cross-slope width $w = 0.680\,\mathrm{m}$, and maximum thickness $T = 0.082\,\mathrm{m}$. Complete details about the analytic definition of the slide shape and the experimental setting can be found at Kirby et al. (2018) and at LTMBW (2017).

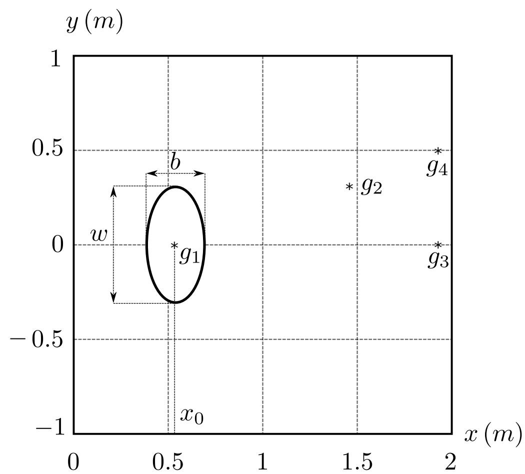

Figure 7: BP2. Sketch of the plan view (case 61 mm). [From Kirby et al. (2018)].

For the numerical simulations, the two-dimensional computational domain $[-1, 10] \times [-1.8, 1.8]$ is considered and discretized with $\Delta x = \Delta y = 0.02\,m$. The number of layers was set to 3. Numerical tests were performed using more layers and similar results were obtained. The CFL number was set to 0.9 and $g = 9.81$. The simulated time was $4\,s$. As boundary conditions, rigid wall conditions were imposed at $y = -1.8,\ y = 1.8$ and outflow conditions at $x = -1,\ x = 10$.

The benchmark test proposed consists in reproducing the slide shape and complete experimental set-up in and using the information about submergence and kinematics to replicate numerically Enet and Grilli's experiments for $d = 61$ and $d = 120$ mm. It is required to simulate surface elevations measured at the four wave gauges (average of 2 replicates of experiments) and present comparisons of the model with the experimental results.

https://doi.org/10.5194/nhess-2020-171
Preprint. Discussion started: 27 August 2020

Enet and Grilli (2007) performed experiments for 7 initial submergence depths d. They are listed in Table 4, together with values of related slide parameters and some measured tsunami wave characteristics. Here, the numerical results corresponding to the two NTHMP required experiments (for $d = 61$ and $d = 120$ mm) will be presented first, then, as data for the seven experiments were provided, the comparison for the remaining five cases will also be presented.

d (mm)	**61**	80	100	**120**	140	149	189
x_g (mm) (measured)	551	617	696	763	846	877	1017
x_g (mm) (theoretical)	560	630	705	780	854	888	1037
η_0 (mm)	13.0	9.2	7.8	5.1	4.4	4.2	3.1
R_u (mm)	6.2	5.7	4.4	3.4	2.3	2.7	2.0
C_m	0.601	0.576	0.627	0.679	0.761	0.601	0.576
C_d	0.473	0.509	0.367	0.332	0.302	0.364	0.353
a_0 (m/s)	1.20	1.21	1.19	1.17	1.14	1.20	1.21
u_t (m/s)	1.70	1.64	1.93	2.03	2.13	1.94	1.97
t_0 (s)	1.42	1.36	1.62	1.74	1.87	1.62	1.63
S_0 (m)	2.408	2.223	3.130	3.522	3.980	3.136	3.207

Table 4: Measured and curve-fitted slide and wave parameters for the 7 experiments performed by Enet and Grilli (2007).

g_1	g_2	g_3	g_4
(x_0,0)	(1469,350)	(1929,0)	(1929,500)

Table 5: Wave gauge locations (x, y) in mm, as shown in Figure 7.

In Figure 8 the comparison of the Multilayer-HySEA model numerical results with measured data for the first case, $d = 61\,mm$, in the four gauges, is presented. An excellent agreement can be observed between these time series. The comparisons for the second required case ($d = 120\,mm$) in the 3 gauges with data provided (gauge g_3 was not available) are shown in Figure 9. Good

https://doi.org/10.5194/nhess-2020-171
Preprint. Discussion started: 27 August 2020

agreement can also be observed in this case. Finally, Figure 10 shows the comparison for the five remaining cases provided by Enet and Grilli. In all cases (for all submergences), a good agreement between simulated results and measured lab data can be observed.

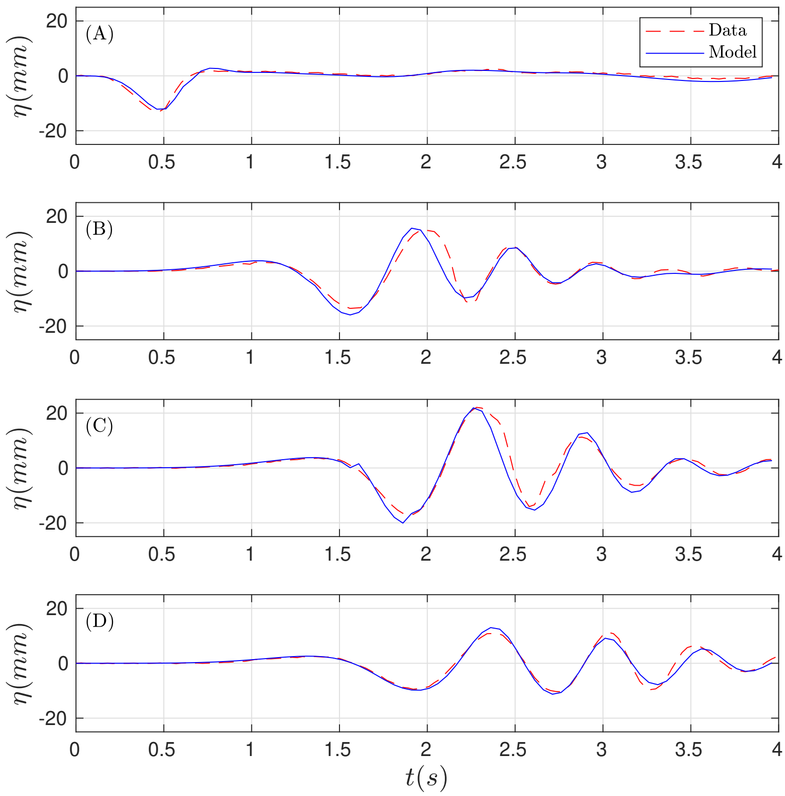

Figure 8: Test case $d = 61\ mm$. Numerically computed (in blue) time time series at wave gauges (A) g_1, (B) g_2, (C) g_3, and (D) g_4 compared with the lab measured data (in red).

https://doi.org/10.5194/nhess-2020-171
Preprint. Discussion started: 27 August 2020

Natural Hazards and Earth System Sciences
Open Access
Discussions

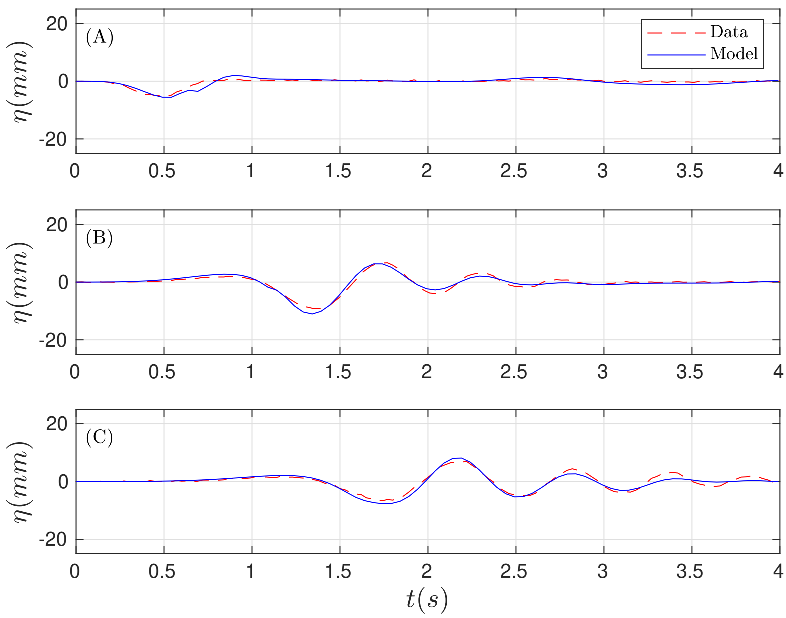

Figure 9: Test case $d = 120\ mm$. Numerically computed (in blue) time time series at wave gauges (A) g_1, (B) g_2, and (C) g_4 for compared with the lab measured data (in red).

https://doi.org/10.5194/nhess-2020-171
Preprint. Discussion started: 27 August 2020

Natural Hazards and Earth System Sciences
Open Access
Discussions

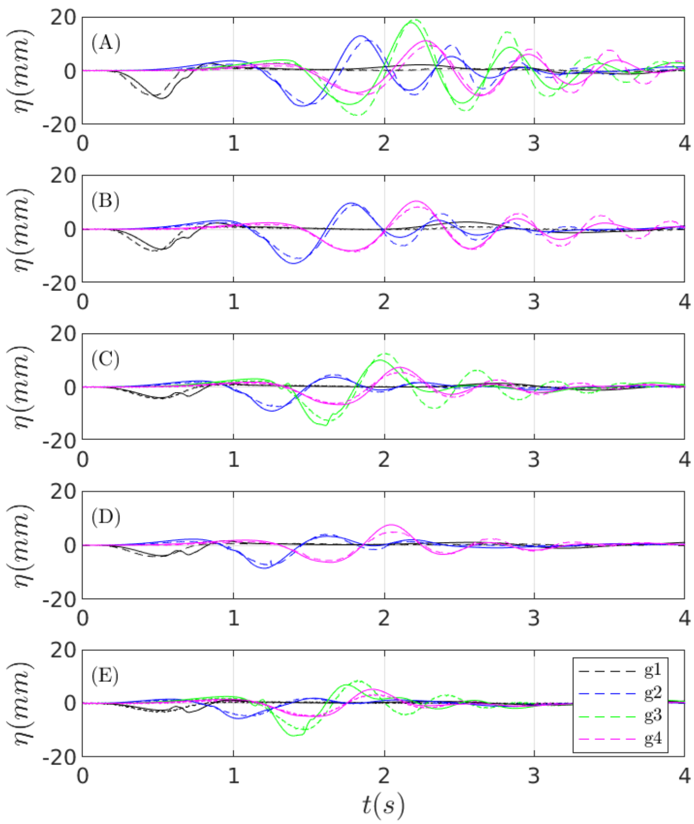

Figure 10: Comparison of data time series (red) and numerical at wave gauges for the cases (A) $d = 80\ mm$, (B) $d = 100\ mm$, (C) $d = 140\ mm$, (D) $d = 149\ mm$, and (E) $d = 189\ mm$.

In Table 6, the execution times for simulations performed on a NVIDIA Tesla P100 GPU are presented. It can be observed that including non-hydrostatic terms in the NLSW equations results in an increase of the computational time in 2.65 times. If a richer vertical structure is considered, then larger computational times are required. As examples for the two and three-layer systems, 3.3 and 4.45 times increase in the computational effort.

	Runtime (s)	Ratio
SWE	23.08	1
1L-NH	61.20	2.65
2L-NH	76.35	3.30
3L-NH	102.93	4.45

Table 6: Execution times in seconds for SWE and non-hydrostatic GPU implementations. Ratios compared with SWE.

Figure 11 shows the comparison, for the four models considered, of the numerical results with the measured data at gauge g_4 for the case $d = 189\ mm$. It can be observed that a model vertical structure considering only one layer is not enough to reproduce the observed data, and that considering 2 and 3 layers in the model produce much better numerical results.

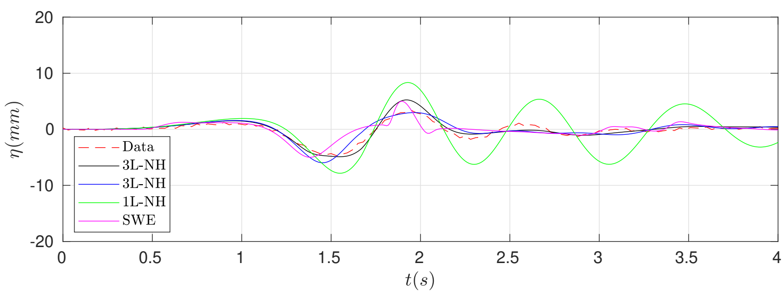

Figure 11: Test case $d = 189\ mm$. Lab measured data (red) and numerically computed time series at wave gauge g_4 using different numerical models.

https://doi.org/10.5194/nhess-2020-171
Preprint. Discussion started: 27 August 2020

5.3. Benchmark Problem 3: Three-dimensional submarine/subaerial triangular solid block

This benchmark problem is based on the 3D laboratory experiment of Wu (2004) and Liu et al. (2005), for a series of triangular blocks of several aspect ratios moving down a plane slope into the water from a dry (subaerial) or wet (submarine) location. Figure 12 shows the schematic description of the set-up for this benchmark in the case of a partially submerged block. Further details can be found at Kirby et al. (2018) and at LTMBW (2017). The laboratory experiments were conducted in a wave tank at Oregon State University of length 104 m, width 3.7 m, and depth 4.6 m.

A plane slope 1:2 (as the one shown in Figure 12 upper panel) with $\theta = 26.6°$ was located near one end of the tank and a dissipating beach in the other. In all the experiments, the water depth was $h_0 = 2.44\,\mathrm{m}$. The experiments retained for the present benchmark were all performed with a triangular block of length $b = 0.91\,\mathrm{m}$, width $w = 0.61\,\mathrm{m}$, and vertical front face $a = b/2 = 0.455\,\mathrm{m}$.

The block movement was provided by means of a polynomial fitting to measured data, giving the horizontal distance as:

$$x_{0,t} = x_{(0,t=0)} + (a\,t^3 + b\,t^2 + c\,t)\,\cos\beta$$

with $\beta = \arctan(1/2)$ and $x_{(0,t=0)} = -2\Delta$. The polynomial coefficients for the two cases proposed are given in Table 7.

Δ	a	b	c
0.10 m	-0.097588	0.759361	0.078776
-0.25 m	-0.085808	0.734798	-0.034346

Table 7: Polynomial coefficients defining slide motion.

For each case, measured free surface elevations for two wave gauges placed at $(x, y) = (1.83, 0)$ (in m) and $(x, y) = (1.2446, 0.635)$, where x is the distance to the initial coastline and y is the distance to the central cross-section (see location at Fig. 12 lower panel). Also measured runup for each case is given at

https://doi.org/10.5194/nhess-2020-171
Preprint. Discussion started: 27 August 2020

runup gauges 2 and 3 in Figure 12 lower panel, lying on the slope at a distance 0.305 m and 0.611 m from the central cross-section, respectively.

The two-dimensional computational domain $[-2, 6] \times [-2, 2]$ is discretised with $\Delta x = 0.04\ m$ and the number of layers was set up to 3. Numerical experiments using more number of layers were performed, obtaining similar results. The stability CFL number was set to 0.9 and $g = 9.81$. The simulated time was 4 s. The same boundary conditions, as in the previous case, were imposed. In order to capture turbulent processes, as in benchmark 1, the complete Navier-Stokes viscous stress tensor is used with the same sub-grid model and coefficients.

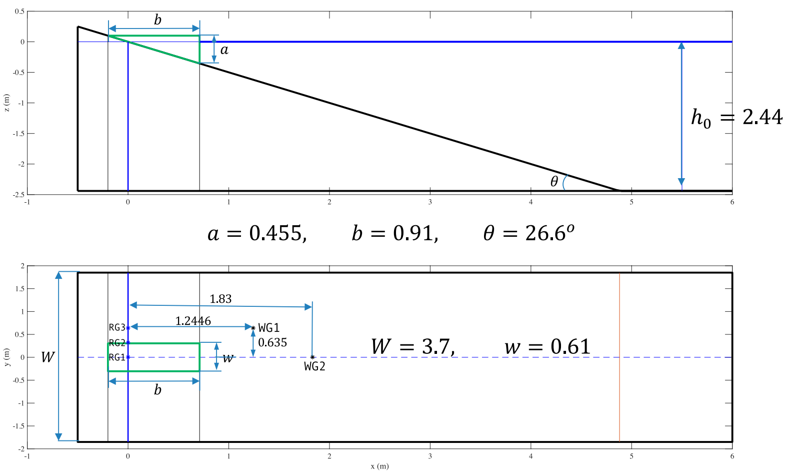

Figure 12: Definition sketch for BP3 laboratory experiments. Here for a submerged ($\Delta < 0$) slide. Upper panel vertical cross section, lower panel plan view.

The numerical results obtained for the subaerial test case are presented in Figures 13 and 14. Figure 13 depicts the comparison for the time series at the wave gauges and Figure 14 at the runup gauges. The same comparison has been performed for the submerged test case, and it is presented in Figures 15 and 16. The agreement for the wave gauges is quite good for WG1 in both cases. For WG2, just in front of the block, an overshoot after the first depression wave is

https://doi.org/10.5194/nhess-2020-171
Preprint. Discussion started: 27 August 2020

observed in both cases. For the run-up, the qualitative agreement is quite good, with the larger discrepancies in RG3 for the submarine test case.

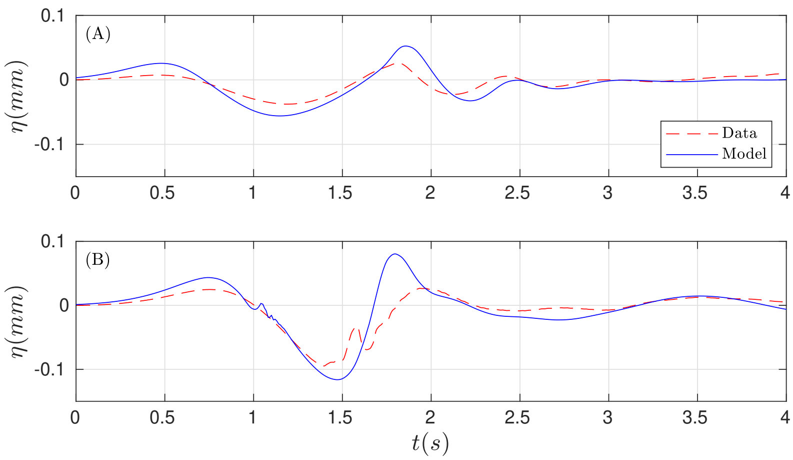

Figure 13: Subaerial test case. Lab measured water height (red) and numerical time series (blue) at wave gauges (A) WG1 and (B) WG2 .

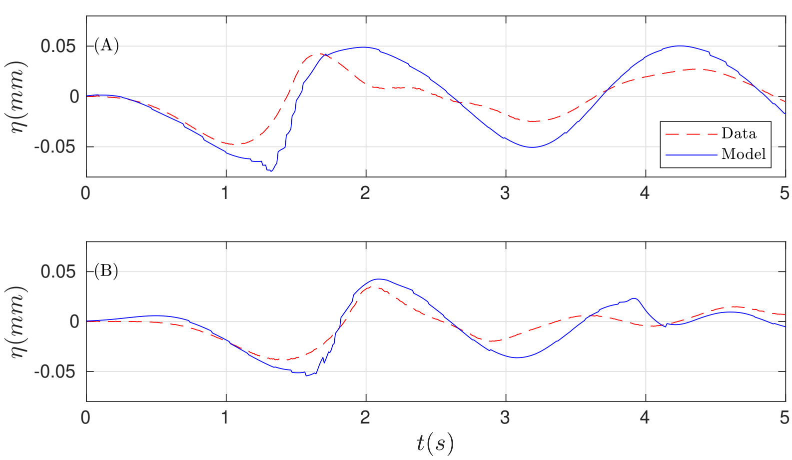

Figure 14: Subaerial test case. Lab measured runup (red) and numerical time series (blue) at runup gauges (A) RG2 and (B) RG3.

https://doi.org/10.5194/nhess-2020-171
Preprint. Discussion started: 27 August 2020

Natural Hazards and Earth System Sciences
Open Access
Discussions

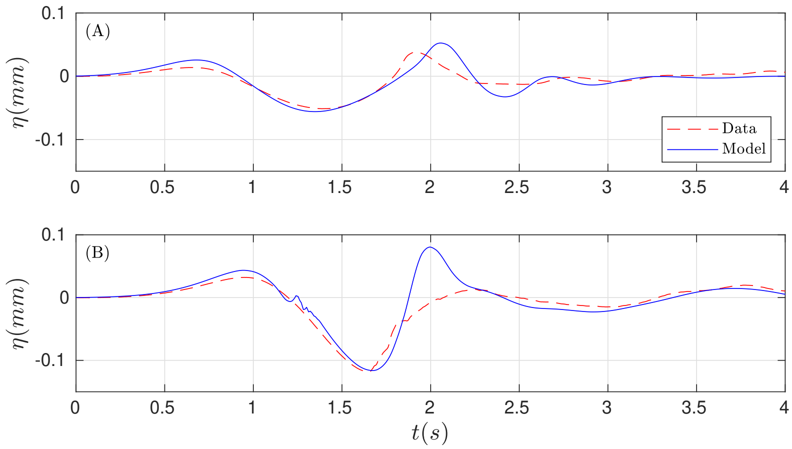

Figure 15: Submerged test case. Lab measured water height (red) and numerical time series (blue) at wave gauges (A) WG1 and (B) WG2.

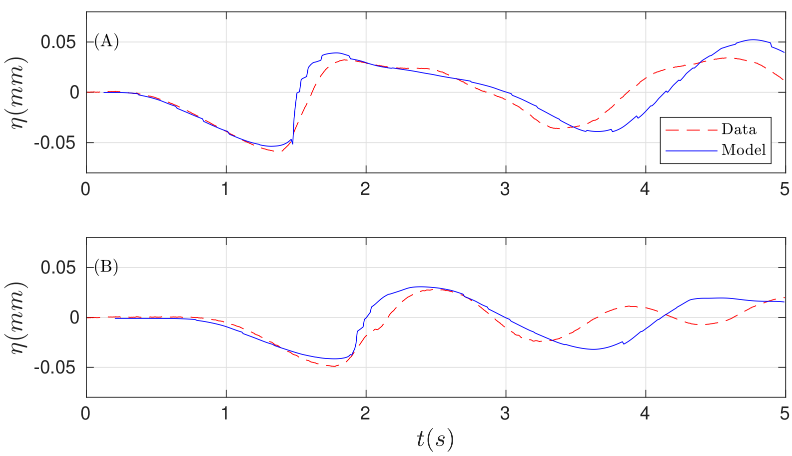

Figure 16: Submerged test case. Lab measured runup (red) and numerical time series (blue) at runup gauges (A) RG2 and (B) RG3.

https://doi.org/10.5194/nhess-2020-171
Preprint. Discussion started: 27 August 2020

6. Concluding Remarks

Validation of numerical models is a first unavoidable step before their use as predictive tools. This requirement is even more necessary when the developed models are going to be used for risk assessment in natural events where human lives are involved. The present work is the first step in this task for the Multilayer-HySEA model, a novel dispersive multilayer model of the HySEA suite developed at the University of Malaga. This model considers a stratified vertical structure and includes non-hydrostatic terms, this is done in order to include the dispersive effects in the propagation of the waves in a homogeneous, inviscid, and incompressible fluid. The numerical scheme implemented, combines a highly robust and efficient finite volume path-conservative scheme for the underlying hyperbolic system and finite differences for the discretization of the non-hydrostatic terms. In order to increase numerical efficiency, the numerical model is implemented to run in GPU architectures. In particular in NVIDIA graphics cards and using CUDA language. In the case of the traditional SW non-dispersive model, this kind of implementations produces an extremely efficient and fast code (Macías et al., 2020d). Increasing the number of layers in SW models provides an enhanced vertical resolution and, at the same time, increases the computational cost. Despite this, from a computational point of view, the two-layer non-hydrostatic code presents a good computational efficiency, and computing times with respect to the one-layer SWE GPU code are absolutely reasonable, being only from 2 to 2.5 larger that for the one layer case. In the numerical simulations performed in the present work, the non-hydrostatic wall-clock times are always below 4.45 times those for the traditional SWE HySEA model, for a number of vertical layers up to three. The numerical scheme presented here and the corresponding multilayer SW water model proposed, is highly efficient and is able to model dispersive effects with a low computational cost.

Regarding model results, they show a good agreement with the experimental data for the three benchmark problems studied in the present work. In partic-

https://doi.org/10.5194/nhess-2020-171
Preprint. Discussion started: 27 August 2020

ular, for BP2, but this also occurs for the other two benchmark problems, we have shown that a one-layer, hydrostatic or non-hydrostatic, model is not able to reproduce the complexity in the observed lab data considered in the proposed benchmarks. The waves to be modeled in the test cases proposed here are high-frequency and dispersive. Hence, it is at least necessary a two-layer structure and non-hydrostatic terms in the model to be used in order to capture the dynamics of the generated waves. As pointed out in Kirby et al. (2018), non-hydrostatic multilayer models, like the one used here, can perform as well as Navier-Stokes equation models but at much lower computational cost as has been shown here.

7. Code and data availability

The numerical code is currently under development and only available to close collaborators. In the future, we will provide an open version of the code as we already do for Tsunami-HySEA. This version will be downloaded from https://edanya.uma.es/hysea/index.php/download.

All the data used in the present work and necessary to reproduce the experiments set-up of the numerical experiments and the laboratory measured data to compared with, can be downloaded from LTMBW (2017) at the web site http://www1.udel.edu/kirby/landslide/. Finally, the NetCDF files containing the numerical results obtained with the Multilayer-HySEA code can be found and download from Macías et al. (2020b).

8. Authors' contributions

JM is leading the HySEA codes benchmarking effort undertaken by the EDANYA group, he wrote most of the paper, reviewed and edited it, assisted in the numerical experiments and in their set up. CE implemented the numerical code and performed all the numerical experiments, he also contributed to writing the manuscript. JM and CE did all the figures. MC strongly contributed to the design and implementation of the numerical code.

https://doi.org/10.5194/nhess-2020-171
Preprint. Discussion started: 27 August 2020

Natural Hazards and Earth System Sciences
Open Access
Discussions

9. Competing interest

The authors declare that they have no conflict of interest.

10. Acknowledgements

This research has been partially supported by the Spanish Government-FEDER funded project MEGAFLOW (RTI2018-096064-B-C21), the Junta de Andalucía-FEDER funded project UMA18-Federja-161 and the University of Málaga, Campus de Excelencia Internacional Andalucía Tech.

References

Adsuara, J., Cordero-Carrión, I., Cerdá-Durán, P., Aloy, M., 2016. Scheduled relaxation Jacobi method: Improvements and applications. Journal of Computational Physics 321, 369–413.

Ataie-Ashtiani, B., Najafi-Jilani, A., 2008. Laboratory investigations on impulsive waves caused by underwater landslide. Coastal Engineering 55 (12), 989 – 1004.

Bai, Y., Cheung, K. F., 2018. Linear shoaling of free–surface waves in multi–layer non–hydrostatic models. Ocean Modelling 121, 90 – 104.

Castro, M., Ortega, S., de la Asunción, M., Mantas, J., Gallardo, J., 2011. GPU computing for shallow water flow simulation based on finite volume schemes. Comptes Rendus Mécanique 339 (2–3), 165–184.

Cui, H., Pietrzak, J., Stelling, G., 2014. Optimal dispersion with minimized Poisson equations for non–hydrostatic free surface flows. Ocean Modelling 81, 1 – 12.

de la Asunción, M., Castro, M., González-Vida, J., Macías, J., Ortega, S., Sánchez-Linares, C., 2013. East coast non-seismic tsunamis: A first landslide approach. Tech. rep., NOAA report.

Enet, F., Grilli, S., 2007. Experimental study of tsunami generation by three-dimensional rigid underwater landslides. Journal of Waterway, Port, Coastal, and Ocean Engineering 133 (6), 442–454.

Escalante, C., Fernández-Nieto, E., Morales, T., Castro, M., 2018a. An efficient two–layer non–hydrostatic approach for dispersive water waves. Journal of Scientific Computing.

Escalante, C., Morales, T., Castro, M., 2018b. Non-hydrostatic pressure shallow flows: GPU implementation using finite volume and finite difference scheme. Applied Mathematics and Computation 338, 631 – 659.

Fernández, E., Bouchut, F., Bresh, D., Castro, M., Mangeney, A., 2008. A new Savage-Hutter type model for submarine avalanches and generated tsunami. J. Comp. Phys. 227, 7720–7754.

Fernández-Nieto, E., Castro, M., Parés, C., 2011. On an intermediate field capturing Riemann solver based on a parabolic viscosity matrix for the two-layer shallow water system. Journal of Scientific Computing 48 (1–3), 117–140.

Fernández-Nieto, E., Parisot, M., Penel, Y., Sainte-Marie, J., 2018. A hierarchy of dispersive layer-averaged approximations of Euler equations for free surface flows. Communications in Mathematical Sciences 16 (5), 1169–1202.

Fritz, D., Hager, W., Minor, H.-E., 2001. Lituya Bay case: rockslide impact and wave runup. Science of Tsunami Hazards 19(1), 3–22.

González-Vida, J., Macías, J., Castro, M., Sánchez-Linares, C., Ortega-Acosta, S., Arcas, D., 2019. The Lituya Bay landslide-generated mega-tsunami. Numerical simulation and sensitivity analysis. Nat. Hazards Earth Syst. Sci. 19 (2), 369–388.

Grilli, S., Vogelmann, S., Watts, P., 2002. Development of a 3D numerical wave tank for modeling tsunami generation by underwater landslides. Engineering Analysis with Boundary Elements 26 (4), 301 – 313.

https://doi.org/10.5194/nhess-2020-171
Preprint. Discussion started: 27 August 2020

Natural Hazards and Earth System Sciences
Open Access
Discussions

Grilli, S., Watts, P., 1999. Modeling of waves generated by a moving submerged body. applications to underwater landslides. Engineering Analysis with Boundary Elements 23 (8), 645 – 656.

Grilli, S., Watts, P., 2005. Tsunami generation by submarine mass failure. I: Modeling, experimental validation, and sensitivity analyses. Journal of Waterway, Port, Coastal, and Ocean Engineering 131 (6), 283–297.

Heller, V., Hager, W., 2011. Waves types of landslide generated impulse waves. Ocean Engineering 38 (4), 630–640.

Horrillo, J., Grilli, S., Nicolsky, D., Roeber, V., Zhang, J., Mar 2015. Performance benchmarking tsunami models for NTHMP's inundation mapping activities. Pure and Applied Geophysics 172 (3), 869–884.

Iglesias, O., 2015. Generación y propagación de tsunamis en el mar catalano-balear. Ph.D. thesis, Universitat de Barcelona, [http:/hdl.handle.net/2445/68704].

Kirby, J., Grilli, S., Zhang, C., Horrillo, J., Nicolsky, D., Liu, P. L.-F., 2018. The NTHMP landslide tsunami benchmark workshop, Galveston, January 9-11, 2017. Tech. rep., Research Report CACR-18-01.

Liu, P. L.-F., Wu, T.-R., Raichlen, F., Synolakis, C. E., Borrero, J. C., 2005. Runup and rundown generated by three-dimensional sliding masses. Journal of Fluid Mechanics 536, 107144.

LTMBW, 2017. Landslide Tsunami Model Benchmarking Workshop, Galveston,Texas, 2017. `http://www1.udel.edu/kirby/landslide/index.html`, accessed: 2020-04-25.

Lynett, P., Gately, K., Wilson, R., Montoya, L., Arcas, D., Aytore, B., Bai, Y., Bricker, J., Castro, M., Cheung, K., David, C., Dogan, G., Escalante, C., González-Vida, J., Grilli, S., Heitmann, T., Horrillo, J., Kanouglu, U., Kian, R., Kirby, J., Li, W., Macías, J., Nicolsky, D., Ortega, S., Pampell-Manis, A.,

https://doi.org/10.5194/nhess-2020-171
Preprint. Discussion started: 27 August 2020

Natural Hazards and Earth System Sciences
Open Access
EGU
Discussions

Park, Y., Roeber, V., Sharghivand, N., Shelby, M., Shi, F., Tehranirad, B., Tolkova, E., Thio, H., Velioglu, D., Yalciner, A., Yamazaki, Y., Zaytsev, A., Zhang, Y., 2017. Inter-model analysis of tsunami-induced coastal currents. Ocean Modelling 114, 14 – 32.

Lynett, P., Liu, P. L.-F., 2002. A numerical study of submarine–landslide–generated waves and run–up. Proceedings of the Royal Society of London A: Mathematical, Physical and Engineering Sciences 458 (2028), 2885–2910.

Lynett, P., Liu, P. L.-F., 2004. A two–layer approach to wave modelling. Proceedings of the Royal Society of London A: Mathematical, Physical and Engineering Sciences 460 (2049), 2637–2669.

Ma, G., Shi, F., Kirby, J., 2012. Shock-capturing non-hydrostatic model for fully dispersive surface wave processes. Ocean Modelling 43–44, 22–35.

Macías, J., Castro, M., Ortega, S., Escalante, C., González-Vida, J., Jun 2017. Performance benchmarking of Tsunami-HySEA model for NTHMP's inundation mapping activities. Pure and Applied Geophysics.

Macías, J., Escalante, C., Castro, M., 2020a. Multilayer-HySEA model validation for landslide generated tsunamis. Part II Granular slides. Submitted to Nat. Hazards Earth Syst. Sci.

Macías, J., Escalante, C., Castro, M., 2020b. Numerical results in Multilayer-HySEA model validation for landslide generated tsunamis. Part I Rigid slides. Dataset on Mendeley, doi: 10.17632/xtfzrbvcb2.1.

Macías, J., Escalante, C., Castro, M., 2020c. Performance assessment of Tsunami-HySEA model for NTHMP tsunami currents benchmarking. laboratory data. Coastal Engineering 158 (103667).

Macías, J., Escalante, C., Castro, M., González-Vida, J., Ortega, S., 2017. HySEA model. landslide benchmarking results. Tech. rep., In NTHMP report.

https://doi.org/10.5194/nhess-2020-171
Preprint. Discussion started: 27 August 2020

Macías, J., Ortega, S., González-Vida, J., Castro, M., 2020d. Performance assessment of Tsunami-HySEA model for NTHMP tsunami currents benchmarking. field cases. Ocean Modeling 152, 101645.

Macías, J., Vázquez, J., Fernández-Salas, L., González-Vida, J., Bárcenas, P., Castro, M., del Río, V. D., Alonso, B., 2015. The Al-Borani submarine landslide and associated tsunami. A modelling approach. Marine Geology 361, 79 – 95.

Madsen, P., Sorensen, O., 1992. A new form of the Boussinesq equations with improved linear dispersion characteristics. Part 2: A slowing varying bathymetry. Coastal Engineering 18, 183–204.

Sánchez-Linares, C., 2011. Simulación numérica de tsunamis generados por avalanchas submarinas: aplicación al caso de Lituya Bay. Master's thesis, University of Málaga, Spain.

Schäffer, H. A., Madsen, P. A., 1995. Further enhancements of Boussinesq–type equations. Coastal Engineering 26 (1), 1 – 14.

ten Brink, U., Chaytor, J., Geist, E., Brothers, D., Andrews, B., 2014. Assessment of tsunami hazard to the U.S. Atlantic margin. Marine Geology 353, 31 – 54.

Watts, P., Grilli, S. T., Kirby, J. T., Fryer, G. J., Tappin, D. R., 2003. Landslide tsunami case studies using a Boussinesq model and a fully nonlinear tsunami generation model. Natural Hazards and Earth System Sciences 3 (5), 391–402.

Watts, P., Grilli, S. T., Tappin, D. R., Fryer, G. J., 2005. Tsunami generation by submarine mass failure. II: Predictive equations and case studies. Journal of Waterway, Port, Coastal, and Ocean Engineering 131 (6), 298–310.

Wu, T.-R., 2004. A numerical study of three-dimensional breaking waves and turbulence effects. Ph.D. thesis, Cornell University.